Zaher (Zak) M. Kassas, Joe Khalife,
Kimia Shamaei, and Joshua Morales

I Hear, Therefore I Know Where I Am

Compensating for GNSS limitations with cellular signals

©ISTOCKPHOTO.COM/COFOTOISME

Global navigation satellite systems (GNSSs) have been the prevalent positioning, navigation, and timing technology over the past few decades. However, GNSS signals suffer from four main limitations:

1) They are extremely weak and unusable in certain environments (e.g., indoors and deep urban canyons) [1].
2) They are susceptible to unintentional interference and intentional jamming [2], [3].
3) Civilian signals are unencrypted, unauthenticated, and specified in publicly available documents, making them spoofable (i.e., hackable) [3].
4) Their position estimate suffers from a large vertical estimation uncertainty due to the lack of GNSS space vehicle (SV) angle diversity, which is particularly problematic for aerial vehicles [4].

As such, standalone GNSSs will not deliver the stringent demands of future systems such as autonomous vehicles, intelligent transportation systems, and location-based services. Research over the past few years has revealed the potential of signals of opportunity as an alternative or a complement to GNSSs. Signals of opportunity are ambient signals not intended for positioning, navigation, and timing, such as cellular, AM/FM radio, satellite communication, digital television, and Wi-Fi. Among these signals, cellular signals are particularly attractive due to their abundance, geometric diversity, high carrier frequency, large bandwidth, and high received power.

This article presents a multisignal software-defined receiver (SDR) architecture for navigating with cellular code division multiple access (CDMA) and long-term evolution (LTE) signals. When GNSS signals are unavailable or compromised, the SDR extracts navigation observables from cellular signals, producing a navigation solution in a standalone fashion. When GNSS signals are available, the cellular navigation observables are fused with GNSS observables, yielding a superior navigation solution to a standalone GNSS solution. Exploiting the abundant cellular signals in the environment provides a more robust and accurate navigation solution.

Digital Object Identifier 10.1109/MSP.2017.2715363
Date of publication: 6 September 2017

Evolution of radion navigation

Radio navigation has come a long way since its inception in the early 1900s when the German companies Telefunken and Lorenz started constructing radio beacon systems (or *Funkbaken*) in 1907. Circular radio beacons were set up in 1921 in the United States for maritime navigation. Then, in 1928, a low-frequency four-course radio range was introduced in the United States for instrument flying. In 1932, the first aircraft instrument landing system (or *Bordfunkgeraete*) was demonstrated in Germany, with the Lorenz beam using a very-high-frequency (VHF) transmitter. In 1940, the British Gee system, which used a chain of terrestrial stations, was first tested. The Gee system inspired the Americans to construct their long-range navigation (LORAN) system, which went live in 1942. Around that same time period, the Decca system was invented in the United States independently of the Gee system and offered better accuracy for navigating ships and aircrafts. It was later developed in the United Kingdom and became operational in 1944. In 1957, the Soviet Union launched the first satellite, *Sputnik I*. Inspired by the Doppler shifts observed from *Sputnik I,* the United States started developing in 1958 Transit (or NAVSAT), the first global satellite-based navigation system. Transit was realized with a nominal constellation of five satellites, but only one satellite was visible at a time, meaning that a user waited 35–100 min (depending on the latitude) between successive satellite passes to determine its position. The first global, continuously available radio navigation system was the ground-based system Omega, which was developed by the United States and six partner nations. Omega became operational in 1971, enabling ships and aircrafts to determine their position with a two-dimensional (2-D) root-mean square (RMS) accuracy of 2–4 km, by receiving very-low-frequency (VLF) radio signals transmitted by a network of fixed terrestrial radio beacons transmitting at about 10 kW.

Transit's success prompted the U.S. Navy and U.S. Air Force to develop parallel programs in the 1960s, which were eventually combined into one program: Navigation System with Timing and Ranging (or NAVSTAR), which later became known as the global positioning system (GPS). The nominal GPS constellation consists of 24 SVs in medium-earth orbit, the first of which was launched in 1978, and the system was declared operational in 1995. GPS revolutionized position determination over land, sea, air, and even space. The system with its global coverage is available 24 h/day every day, providing the navigator with a highly accurate tool, which operates in all weather conditions. The receiver, on the other hand, is compact and relatively inexpensive, allowing its use by anyone from a hiker to an airplane pilot. The GPS inspired the development of other GNSSs such as the Russian GLONASS (first launched in 1982), the Chinese BeiDou (2000), and the European Galileo (2011) as well as regional navigation satellite systems including the Japanese QZSS (2010) and the Indian IRNSS (2013).

Despite the extraordinary advances in GNSS signal processing and receiver design, GNSSs are unreliable for accurate anytime, anywhere positioning, navigation, and timing due to the four inherent limitations given previously. Traditional approaches to address GNSS limitations have been to fuse GNSS receivers with dead-reckoning systems and map-matching algorithms. These approaches typically fuse the outputs of heterogeneous sensors, particularly inertial navigation systems (INSs), digital map databases, and GNSS receivers, with specialized signal processing algorithms.

Motivated by the plenitude of ambient radio-frequency (RF) signals of opportunity in GNSS-challenged environments, a

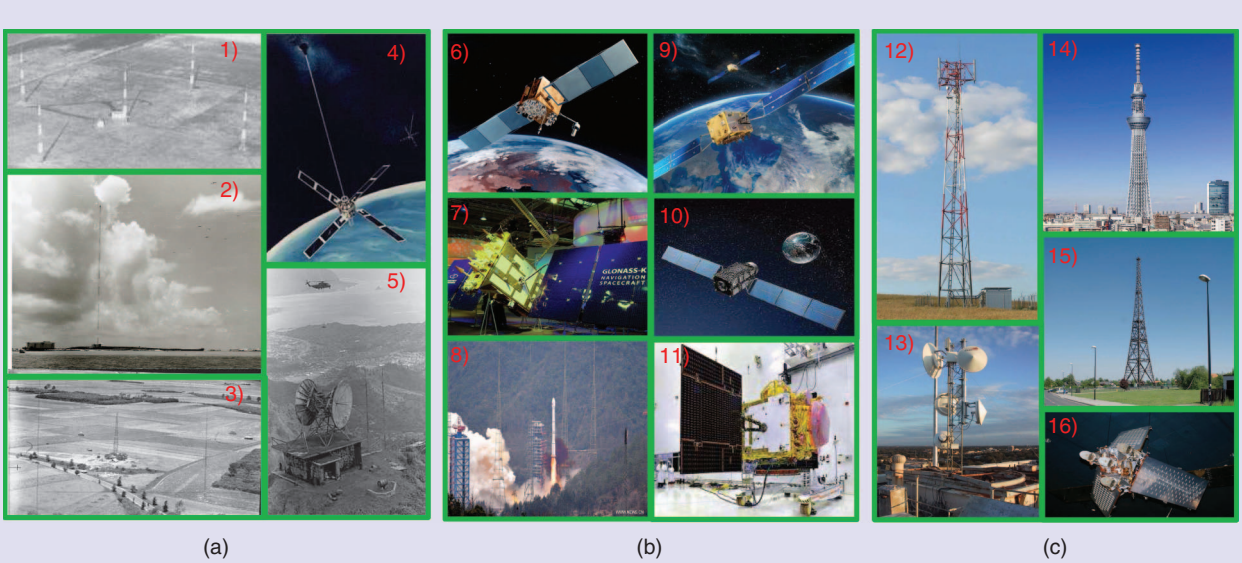

FIGURE 1. The evolution of radio navigation. (a) Early systems: 1) low-frequency four course radio range, 2) LORAN, 3) Gee, 4) Transit, and 5) Omega. (b) Satellite-based navigation systems: 6) GPS, 7) GLONASS, 8) BeiDou (launch), 9) Galileo, 10) QZSS, and 11) IRNSS. (c) Signals of opportunity: 12) cellular, 13) wireless communications access point, 14) digital television, 15) FM, and 16) iridium satellite communication. (Images 1–7 and 12–16 courtesy of www.wikipedia.org. Images 8–11 courtesy of www.insidegnss.com.)

new paradigm to overcome the limitations of GNSS-based navigation has emerged over the past decade [5]. Examples of signals of opportunity include AM/FM radio [6], [7], iridium satellites [8], [9], cellular [10], [11], digital television [12], [13], and Wi-Fi [14], [15]. Figure 1 illustrates various radio navigation transmitters over the past century.

Cellular-based navigation

Among the different signals of opportunity types, cellular signals are particularly attractive due to their following qualities:

- *Abundance*: cellular base transceiver stations (BTSs) are plentiful due to the ubiquity of cellular and smartphones.
- *Geometric diversity*: the cell configuration by construction yields favorable BTS geometry—unlike certain terrestrial transmitters, which tend to be colocated, e.g., digital television.
- *High carrier frequency*: cellular carrier frequency ranges 800–1,900 MHz, which yields precise carrier phase navigation observables.
- *Large bandwidth*: cellular signals have a bandwidth up to 20 MHz (as discussed in the section "LTE"), which yields accurate time-of-arrival (TOA) estimation.
- *High received power*: cellular signals are often available and usable in GNSS-challenged environments—the received carrier-to-noise ratio C/N_0 from nearby cellular BTSs is more than 20 dB-Hz higher than GPS SVs.

Besides the aforementioned advantages, there is no deployment cost associated with using cellular signals for positioning and navigation—the signals are practically free to use. Specifically, the user equipment (UE) could "eavesdrop" on the transmitted cellular signals without communicating with the BTS, extract necessary positioning and timing information from received signals, and calculate the navigation solution locally. While other navigation approaches requiring two-way communication between the UE and BTS (i.e., network based) exist, this article focuses on explaining how UE-based navigation can be achieved with cellular CDMA and LTE signals, presenting receiver architectures that are suitable for software-based implementation (see "Software-Defined Receivers for Navigation") along with ground and aerial vehicle navigation results achieved with these receivers.

CDMA

Cellular CDMA systems employ orthogonal and maximal-length sequences to enable multiplexing over the same channel.

Software-Defined Receivers for Navigation

Software-defined receivers (SDRs) offer many advantages over their hardware-based counterparts, such as 1) flexibility: designs are hardware-independent; 2) modularity: different functions can be implemented independently; and 3) upgradability: minimal changes are needed to improve designs. Signal processing algorithms in SDRs are typically implemented on general-purpose digital signal processors (DSPs), with only minimal dedicated hardware components to the radio-frequency (RF) front end.

Traditionally, baseband operations in GNSS receivers have been implemented using dedicated hardware due to cost, power, and speed. Until recently, GNSS SDRs were limited to postprocessing applications operating on raw samples recorded from an RF front end. However, with modern DSPs, real-time GNSS SDRs are becoming more prevalent [16], [17]. Such SDRs are typically implemented in high-level, textual-based languages, such as C/C++. Processor-specific optimization techniques are often utilized for computationally expensive baseband operations.

Graphical programming languages, such as LabVIEW and Simulink, are attractive choices for implementing navigation SDRs, whether for GNSS or signals of opportunity, for a number of reasons. First, while the optimized C/C++ SDR implementations are often portable and reusable on multicore DSPs, the optimizations required for each processor in real-time applications could slow development and introduce platform-specific errors. Graphical programming languages offer tools that often generate optimized implementations for multiple platforms—desktop, DSP, and field-programmable gate arrays (FPGAs)—without code modifications. Second, navigation SDRs are conceptualized as block diagrams, enabling a one-to-one correspondence between the architectural conceptualization and software implementation. Third, graphical optimized routines are abundant, which could be readily exploitable by navigation SDR designers. Fourth, data-flow-based graphical implementations are easier to understand and debug, and they offer rapid access to all internal signals. Finally, graphical tools provide attractive graphical user interfaces, allowing designers to develop interactive panels that have the look and feel of hardware-based navigation receivers. Graphical implementations of GNSS SDRs [18], [19] and cellular SDRs [20], [21] have been the subject of a number of recent publications.

While SDRs offer many advantages over hardware-based receivers, they suffer from a number of shortcomings: larger size and weight, increased power consumption, and higher cost. This is due to the fact that, unlike hardware-based receivers, SDRs are not optimized for a particular application and they could utilize high-level, general-purpose scripting tools to translate a graphical SDR design into code that gets deployed onto DSPs and FPGAs.

The sequences transmitted on the forward link channel, i.e., from BTS to receiver, are known. Therefore, by correlating the received cellular CDMA signal with a locally generated sequence, the receiver can produce a pseudorange measurement. This technique is used in GPS. With enough pseudorange measurements and knowing the states of the BTSs, the receiver can localize itself within the cellular CDMA environment.

Overview of cellular CDMA forward link structure

In a cellular CDMA communication system, several logical channels are multiplexed on the forward link channel, including a pilot channel, a sync channel, and seven paging channels as described next.

Modulation of forward link CDMA signals

The data transmitted on the forward link channel in cellular CDMA systems are modulated through quadrature phase-shift keying (QPSK) and then spread using direct-sequence CDMA (DS-CDMA). However, the in-phase and quadrature components of the channels of interest carry the same message $m(t)$. The spreading sequences, called the *short code*, are maximal-length pseudorandom noise (PN) sequences that are generated using 15 linear feedback shift registers (LFSRs). Hence, the length of the short code components is $2^{15} - 1 = 32,767$ chips [22]. An extra zero is added after the occurrence of 14 consecutive zeros to make the length of the short code a power of two. To distinguish the received data from different BTSs, each station uses a shifted version of the PN codes. This shift, known as the *pilot offset*, is unique for each BTS and is an integer multiple of 64 chips. Each individual logical channel is spread by a unique 64-chip Walsh code [22]. Spreading by the short code enables multiple access for BTSs over the same carrier frequency, while the orthogonal spreading by the Walsh codes enables multiple access for logical channels over the same BTS.

The CDMA signal is subsequently filtered using a digital pulse-shaping filter that limits the bandwidth of the transmitted CDMA signal according to the CDMA200 standard. The signal is finally modulated by the carrier frequency to produce $s(t)$.

Pilot channel

The message transmitted by the pilot is nothing but the short code. A CDMA receiver utilizes the pilot signal to detect the presence of a CDMA signal and then tracks it. The fact that the pilot signal is dataless allows for longer integration time. The receiver differentiates between the BTSs based on their pilot offsets.

Sync channel

The sync channel is used to provide time and frame synchronization to the receiver. The cellular CDMA system uses GPS as the reference timing source, and the BTS sends the system time as well as the PN offset to the receiver over the sync channel [23].

Paging channel

The paging channel transmits all the necessary overhead parameters for the receiver to register into the network [23]. Some mobile operators also transmit the BTS latitude and longitude on the paging channel, which can be exploited for navigation. The major cellular CDMA providers in the United States (Sprint and Verizon) do not transmit the BTS latitude and longitude. The sync and paging channel structures and the cellular CDMA forward link signal modulator are summarized in Figure 2.

CDMA SDR architecture

The goal of a cellular CDMA receiver is to acquire and track the signal parameters, specifically 1) the code phase or code start time and 2) the carrier phase, which can be constructed from the apparent Doppler frequency. To this end, a CDMA receiver consists of three main stages: signal acquisition, signal tracking, and message decoding.

Acquisition

The objective of this stage is to determine which BTSs are in the receiver's proximity and to obtain a coarse estimate of their corresponding code start times and Doppler frequencies. For a particular PN offset, a search over the code start time and Doppler frequency is performed to detect the presence of a pilot signal. The frequency spacing must be a fraction of the inverse of the integration period, which is 0.08/3 ms if it is assumed to be one PN code period. The code start time search window is naturally chosen to be 0.08/3 ms with a delay spacing of one sample.

Similar to GPS signal acquisition, the search could be implemented either serially or in parallel, which, in turn, could be performed over code phase or Doppler frequency. The proposed receiver performs a parallel code phase search by exploiting the optimized efficiency of the fast Fourier transform (FFT) [24]. If a signal is present, a plot of the squared magnitude of the correlation will show a high peak at the corresponding code start time and Doppler frequency estimates, as shown in Figure 3.

Tracking

After obtaining an initial coarse estimate of the code start time and Doppler frequency of the pilot signal, the receiver refines and maintains these estimates via tracking loops. In the proposed design, a phase-locked loop (PLL) is employed to track the carrier phase, and a carrier-aided delay-locked loop (DLL) is used to track the code phase.

The PLL consists of a phase discriminator, a loop filter, and a numerically controlled oscillator (NCO). Since the receiver is tracking the dataless pilot channel, an `atan2` discriminator, which remains linear over the full input error range of $\pm\pi$, could be used without the risk of introducing phase ambiguities. In contrast, a GPS receiver cannot use this discriminator unless the transmitted data-bit values of the navigation message are known [25]. Furthermore, while GPS receivers require second- or higher-order PLLs due to the high dynamics of GPS SVs, lower-order PLLs could be used in cellular CDMA navigation receivers. The receiver could easily track the carrier phase with a second-order PLL.

The first-order carrier-aided DLL employs the noncoherent dot-product discriminator followed by an amplifier. To compute the code phase error, the dot-product discriminator uses

the prompt, early, and late correlations. The prompt correlation is computed by correlating the received signal with a locally generated PN sequence shifted by the code start time estimate. The early and late correlations are calculated by correlating the received signal with an early and a delayed version of the prompt PN sequence, respectively.

In a GPS receiver, the pseudorange is calculated based on the time a navigation message subframe begins to eliminate ambiguities due to the relative distance between GPS SVs [25]. This necessitates decoding of the navigation message to detect the start of a subframe. These ambiguities do not exist in a cellular CDMA system. This follows from the fact that a PN offset of one translates to a distance greater than 15 km between BTSs, which is beyond the size of a typical cell [26]. The pseudorange can therefore be deduced by multiplying the code start time by the speed of light. Figure 3 shows the receiver architecture along with the intermediate signals produced with a LabVIEW-based implementation of the SDR. Note the C/N_0 of the received cellular CDMA signal (60.8 dB-Hz), which is 15–20 dB higher than that of a typical GPS signal.

Navigation framework and experimental results

By making pseudorange measurements to three or more BTSs, one may estimate the 2-D position and clock bias of a cellular CDMA receiver, provided that the BTS locations and their clock biases are known. Unlike GNSS, the states of cellular CDMA BTSs are unknown to a navigating receiver and need to be estimated. The location of the BTSs can be obtained offline via several methods: 1) accessed from a cellular CDMA BTS location database, 2) surveyed using satellite imagery, or 3) estimated on the fly individually or collaboratively [27], [28]. However, the clock error states of a BTS (clock bias and clock drift) are stochastic and dynamic and therefore must be continuously estimated. A substantial part of the literature on navigation using cellular signals considers positioning with pseudorange measurements; however, certain assumptions such as perfect synchronization or negligible variations between the transmitter and receiver clocks are made to eliminate the clock biases of the BTS and the receiver from the measurement model [29], [30]. Alternatively, clock errors can be calibrated at the beginning by knowing the initial position of the navigator and can be recalibrated over the trajectory when

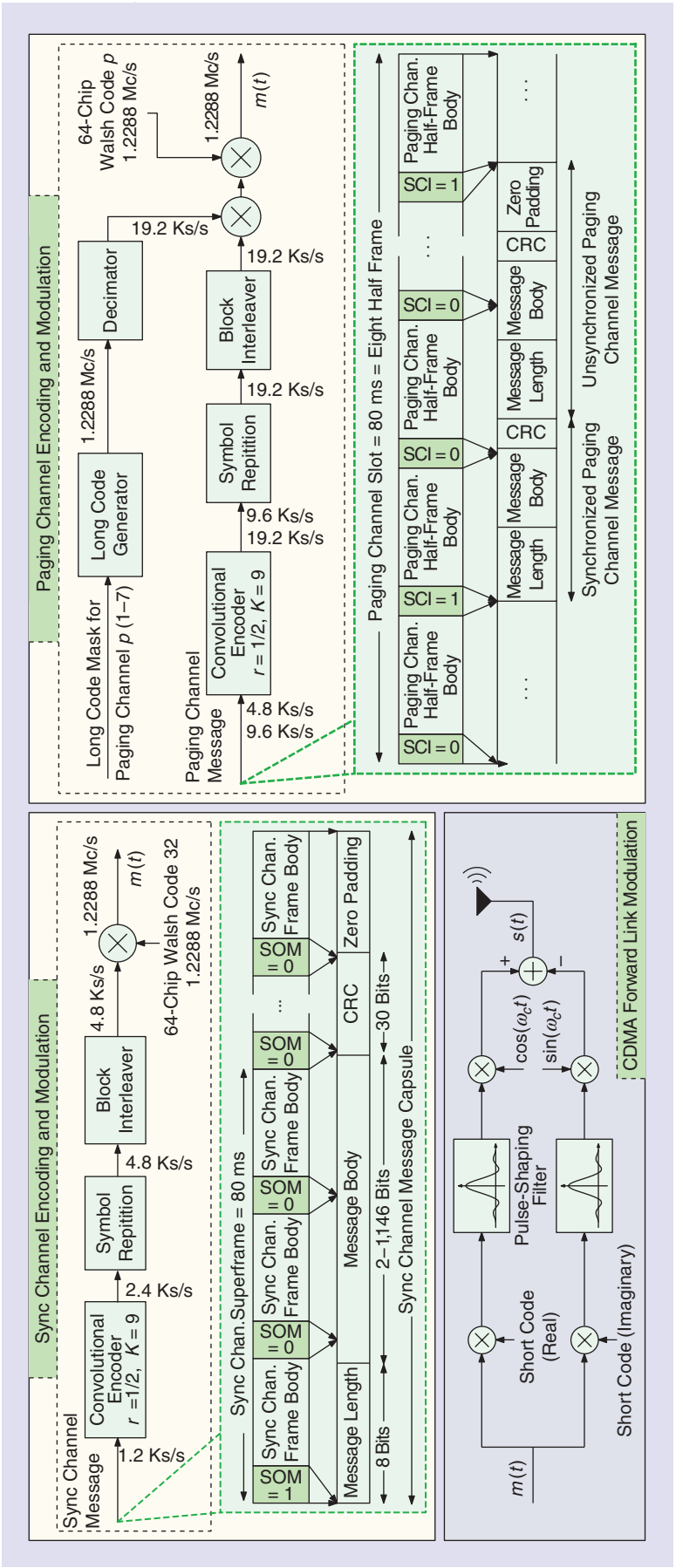

FIGURE 2. Cellular CDMA forward link signal structure.

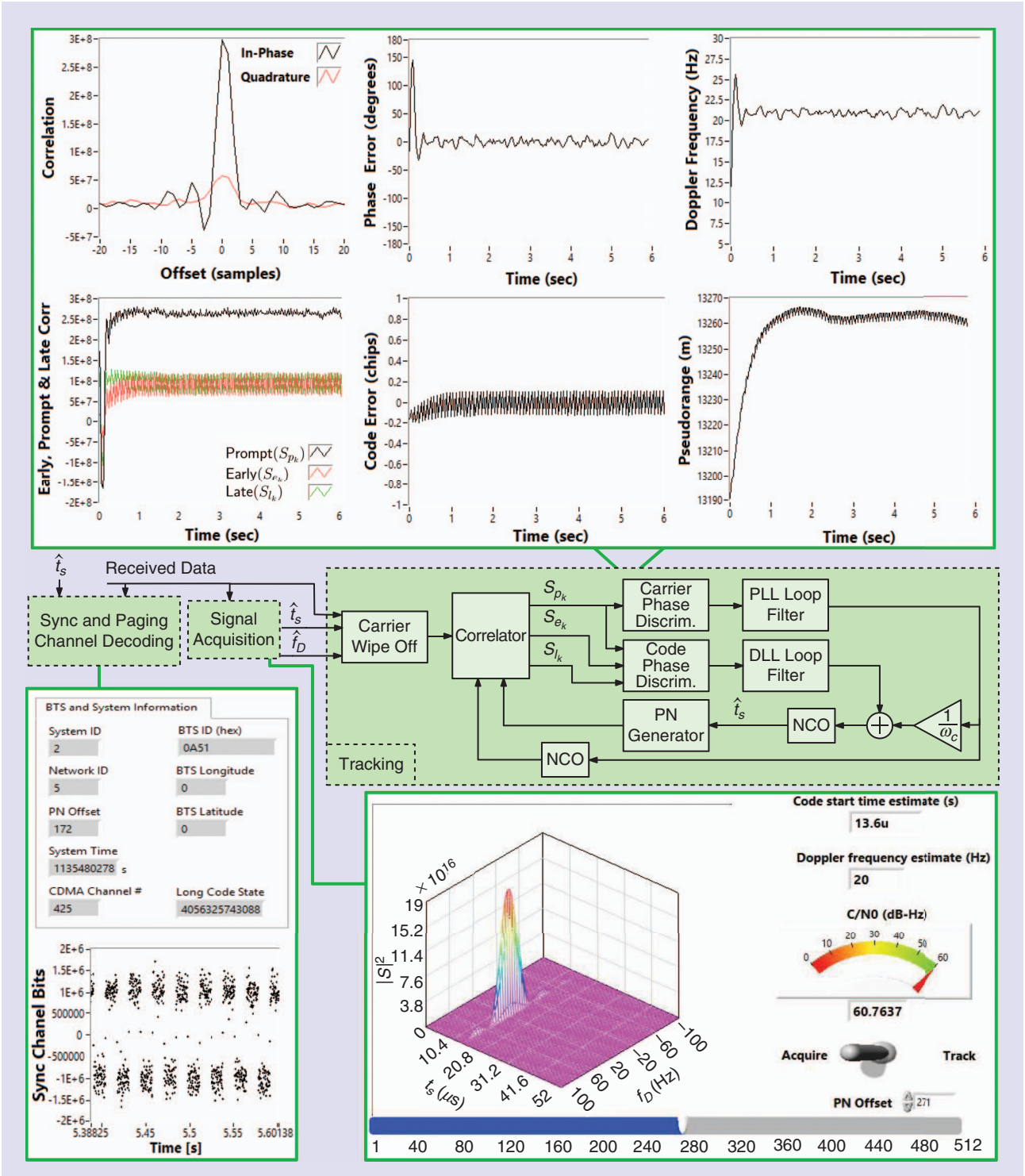

FIGURE 3. A cellular CDMA SDR architecture and LabVIEW front panel showing internal signals: code error; phase error; Doppler frequency; early, prompt, and late correlations; pseudorange; and in-phase and quadrature components of the correlation function.

crossing a known landmark [11]. Other methods rely on monitoring stations or synchronized reference receivers to account for the clock bias of the transmitter [12], [31].

In this article, a navigation framework based on a mapping receiver and a navigating receiver is adopted. Each receiver is equipped with the proposed cellular CDMA SDR. The mapping receiver is assumed to have knowledge of its own position and clock error states (by having access to GNSS signals, for example), to have knowledge of the position of the BTSs, and to be estimating the clock error states of the BTSs. The mapper

shares the BTSs' positions and clock estimates with the navigating receiver, which has no knowledge of its own states. This framework was tested experimentally with the cellular CDMA SDR mounted on a ground vehicle in [20]. Here, this framework is illustrated on an unmanned aerial vehicle (UAV). For this purpose, a stationary mapper and a UAV navigator were equipped with cellular and GPS antennas. The GPS and cellular signals were simultaneously downmixed and synchronously sampled via universal software radio peripherals (USRPs). The GPS signal was processed by a Generalized Radio Navigation Interfusion Device (GRID) SDR [32], and the cellular CDMA signals were processed by the LabVIEW-based SDR proposed in [20]. The ground-truth reference for the navigator trajectory was taken from the UAV's on-board navigation system, which uses GPS, INS, and other sensors.

Over the course of the experiment, the mapper and the navigator were listening to the same two BTSs, of which the position states were mapped prior to the experiment. The mapper was stationary and was estimating the clock bias and drift of the two known BTSs. Since only two BTSs were available for processing, an extended Kalman filter (EKF) framework was adopted (for observability considerations) to estimate the navigator's state. The navigator's position and velocity states were assumed to evolve according to velocity random walk dynamics, and the clock bias and clock drift dynamics were modeled as a double integrator, driven by noise [33]. The navigation framework, experimental setup, and results are summarized in Figure 4.

Figure 4 shows that the trajectory estimated using only cellular CDMA signals follows closely the navigation solution produced by the UAV's onboard navigation system. A closer look at the estimates reveals that most of the errors are along the east direction, which suffers from poor diversity in the BTS geometric

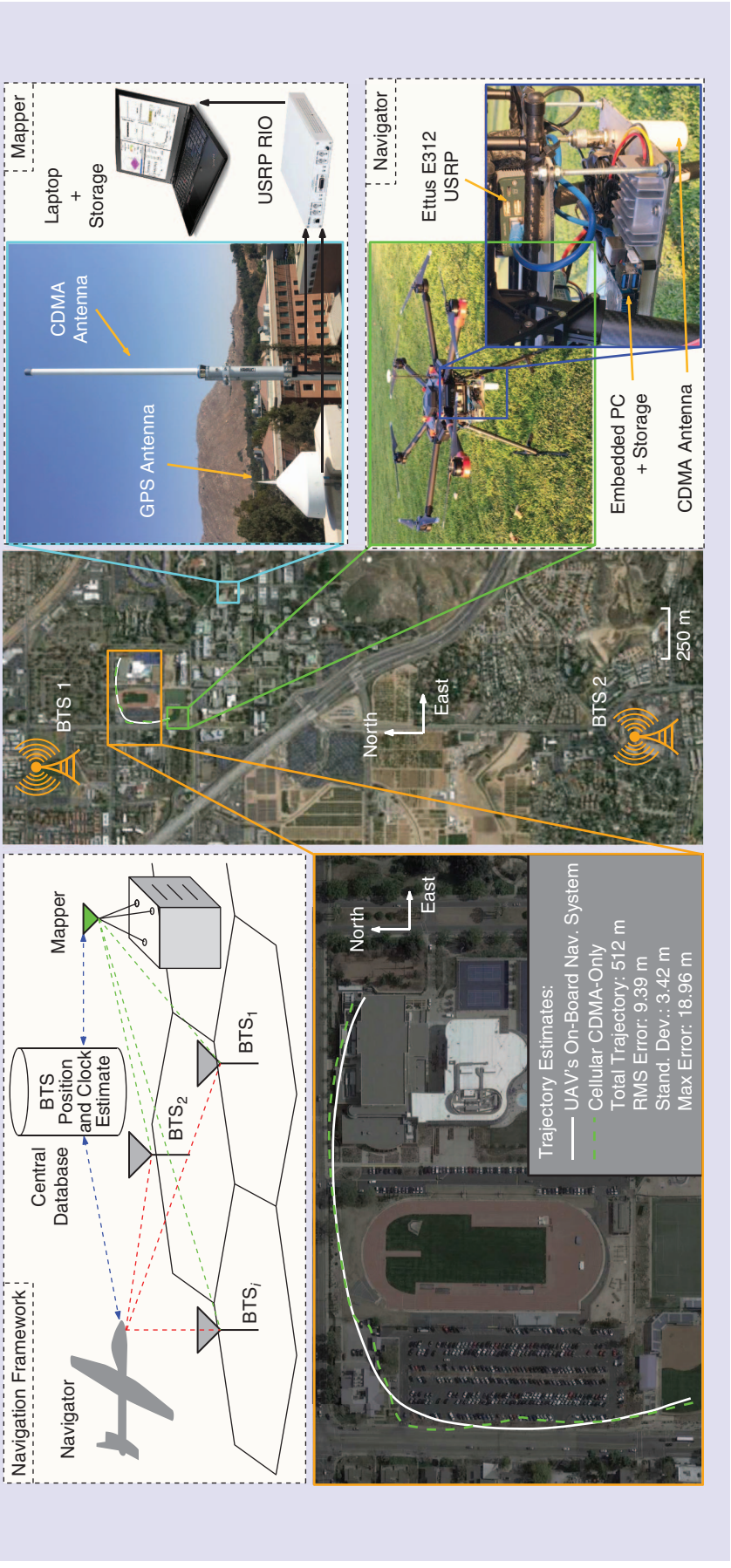

FIGURE 4. The cellular CDMA-based navigation experimental setup and results. Map data courtesy of Google Earth.

configuration. Due to hardware limitations, the USRP onboard the UAV could sample only one cellular CDMA channel at one center frequency, which limits the number of BTSs that are capable of being heard. Moreover, the UAV had a constrained payload, limiting the number of USRPs that could be mounted on the UAV. This limited the number of BTSs used by the navigator (UAV) to two nearby BTSs. With better hardware (e.g., dedicated hardware-based RF front ends) and higher payload capabilities, more BTSs could be simultaneously heard and used to improve the navigation solution.

LTE

In recent years, LTE, the fourth-generation of cellular transmission standard, has received considerable attention for navigation [34]–[40]. This is due to certain desirable characteristics inherent to LTE signals, including 1) higher transmission bandwidth compared to previous generations of wireless standards and 2) the ubiquity of LTE networks. The literature on LTE-based navigation has demonstrated several experimental results for positioning using real LTE signals [36]–[38], [40]. Moreover, several SDRs have been proposed for navigation with real and laboratory-emulated LTE signals [21], [34], [35]. Experimental results with real LTE signals showed meter-level accuracy [21], [41].

Frame structure

In the LTE downlink transmission protocol, the transmitted data are encoded using orthogonal frequency-division multiplexing (OFDM). Figure 5(a) represents the block diagram of the OFDM encoding scheme for a digital transmission. The serial data symbols are first parallelized in groups of length N_r, in which N_r represents the number of subcarriers. Then, each group is zero-padded, and an inverse FFT (IFFT) is taken. Finally, to protect the data from multipath effects, the last L_{CP} elements of the obtained symbols are repeated at the beginning of the data, which is called *cyclic prefix* (*CP*). The transmitted symbols at the receiver can be obtained by executing these steps in reverse order.

The OFDM signals are arranged into multiple blocks, called *frames*. A frame is composed of 10 ms of data, which is divided into 20 slots with a duration of 0.5 ms each, equivalent to ten subframes with a duration of 1 ms each. A slot can be decomposed into multiple resource grids (RGs) and each RG has numerous resource blocks (RBs). An RB is divided into smaller elements—resource elements (REs)—which are the smallest building blocks of an LTE frame. The frequency and time indices of an RE are called *subcarrier* and *symbol*, respectively. The structure of the LTE frame is shown in Figure 5(b) [42].

In the LTE protocol, a reference signal called *positioning reference signal* (*PRS*) is assigned to provide network-based positioning capability. PRS-based positioning suffers from a number of drawbacks: 1) the user's privacy is compromised, since the user's location is revealed to the network [43]; 2) localization services are limited only to paying subscribers and from a particular cellular provider; 3) ambient LTE signals transmitted by other cellular providers are not exploited; and 4) additional bandwidth is required to accommodate the PRS, which caused the majority of cellular providers to choose not to transmit the PRS in favor of dedicating more bandwidth for traffic channels. There are three other sets of reference signals in LTE systems, which can be exploited for positioning purposes. These signals are primary synchronization signal (PSS), secondary synchronization signal (SSS), and cell-specific reference signal (CRS), which are discussed next.

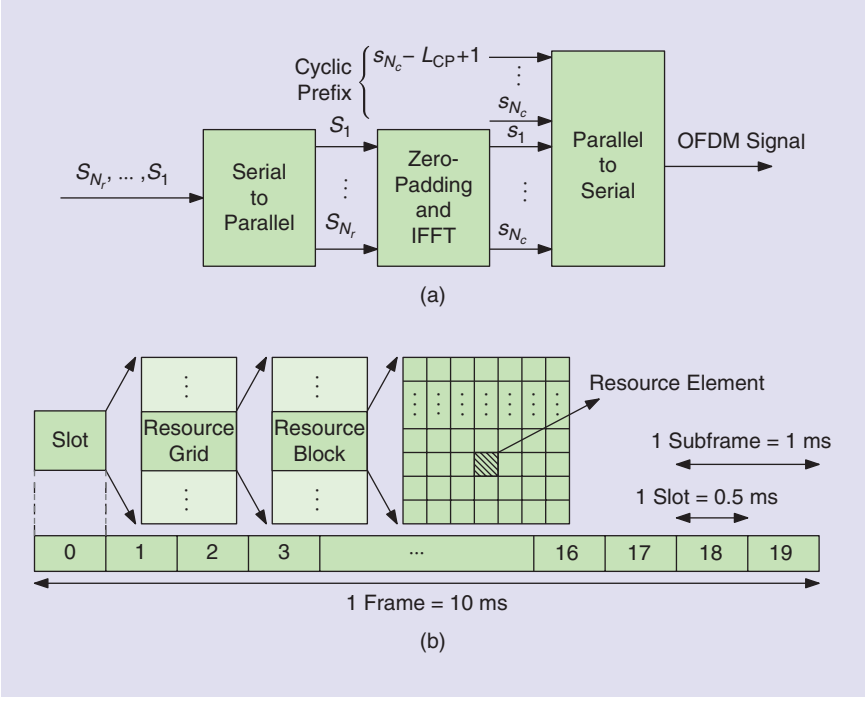

FIGURE 5. (a) An OFDM encoding scheme. (b) An LTE frame structure.

PSS and SSS

When a UE receives an LTE signal, it must reconstruct the LTE frame to extract the relevant information transmitted in the frame. This is achieved by first identifying the frame start time. To determine the frame start time, PSS and SSS are transmitted from each BTS (or eNodeB) and on prespecified symbols and subcarriers of all transmitted frames.

PSS is a Zadoff–Chu sequence of length 62, which is transmitted on the last symbol of slot 0 and repeated on slot 10. SSS is an orthogonal length-62 sequence transmitted in either slot 0 or 10, in the symbol preceding the PSS, and on the same subcarriers as the PSS. SSS is obtained by concatenating two maximal-length sequences scrambled by a third orthogonal sequence generated based on PSS. PSS and SSS map to two integers

representing sector ID and group ID of the eNodeB, respectively. Once the PSS and SSS are detected, the UE can estimate the frame start time, $\hat{t}_s$, and the eNodeB's cell ID.

CRS

The CRS is a pseudorandom sequence, which is uniquely defined by the eNodeB's cell ID. It is spread across the entire bandwidth and is transmitted mainly to estimate the channel frequency response. The CRS subcarrier allocation depends on the cell ID, and it is designed to keep the interference with CRSs from other eNodeBs to a minimum. Since CRS is transmitted throughout the bandwidth, it can accept up to 20 MHz bandwidth.

LTE SDR architecture

To obtain the pseudorange to each eNodeB, the UE must execute several steps: 1) acquisition, 2) system information extraction, 3) tracking, and 4) timing information extraction. These steps are summarized in Figure 6 and are discussed next.

Acquisition

After receiving the LTE signal and downmixing to baseband [Figure 6(a)], the first step in a receiver is to acquire an initial estimate of frame start time and Doppler frequency. By correlating the locally generated PSS and SSS with the received signal, the frame timing is obtained. Figure 6(b) shows the correlation results of PSS and SSS with a real LTE signal. Next, the Doppler frequency is estimated using the received signal and its CP [44]. The block diagram of the acquisition step is presented in Figure 6(c).

System information extraction

Relevant parameters for navigation purposes including the system bandwidth, number of transmitting antennas, and neighboring cell IDs are provided to the UE in two blocks, a master information block (MIB) and system information block (SIB). The receiver must decode the data of several transmitted physical channels to be able to extract relevant navigation information. These channels include 1) physical control format indicator channel (PCFICH), 2) physical downlink control channel (PDCCH), and 3) physical downlink shared channel (PDSCH). These steps are presented in Figure 6(d).

Tracking

After acquiring the LTE frame timing and extracting the relevant navigation information from the received signal, a UE must continue tracking the frame timing for two reasons: 1) to produce a pseudorange measurement and 2) continuously reconstruct the frame. In the tracking architecture shown in Figure 6(e), SSS is exploited for tracking the frame timing. The components of the tracking loops are a frequency-locked loop (FLL)-assisted PLL and a carrier-aided DLL.

The main components of an FLL-assisted PLL are a phase discriminator, a phase loop filter, a frequency discriminator, a frequency loop filter, and a numerically controlled oscillator (NCO). The reference signal SSS is not modulated with other data. Therefore, an `atan2` discriminator, which remains linear over the full input error range of $\pm\pi$, could be used without the risk of introducing phase ambiguities.

In the DLL, the prompt, early, and late correlations are calculated by correlating the received signal with a prompt, early, and delayed versions of the SSS sequence, respectively. The objective of the DLL is to track the null of the S-curve, which is the difference between the early and late correlations. Figure 6(f) shows the tracking results.

Timing information extraction

The SSS code start time estimated in the tracking loop is used to reconstruct the transmitted LTE frame. In LTE systems, PSS and SSS are transmitted with the lowest possible bandwidth. Consequently, the timing resolution obtained from these signals is low. To achieve higher localization precision, CRS can be exploited. First, the channel impulse response is estimated using CRS. Then, the TOA is estimated by using the first peak of the estimated channel impulse response. This step is presented in Figure 6(g), and the obtained pseudorange is shown in Figure 6(h).

Navigation framework and experimental results

Different methods to extract LTE pseudorange have been proposed. The estimation of signal parameters via rotational invariance technique is used in [40] to extract the pseudorange, which provides accurate results but is complex to implement. An SDR that tracks CRS exclusively, which has lower complexity compared to the LTE SDR discussed in this article, was proposed in [34]. However, it has lower precision, since it tracks the maximum of the channel impulse response amplitude; therefore, the precision is limited to the bandwidth of the CRS.

It is commonly assumed in the literature that the receiver has knowledge of the eNodeB's clock error [34] or that the receiver solves for the clock error and removes it by postprocessing [21], [36], [40]. In this article, an EKF is used to estimate the UE's position and velocity states and the difference between the UE's clock bias and eNodeBs' and between the UE's clock drift and the eNodeBs'. The UE's position and velocity states were assumed to evolve according to velocity random walk dynamics, and the clock bias and clock drift dynamics were modeled as a double integrator, driven by noise [33]. The eNodeBs' positions are assumed to be known to the UE. Also, the UE had knowledge of its own initial position, velocity, clock bias, and clock drift (from GPS) before it started navigating with LTE signals.

To evaluate the performance of the LTE SDR, a field test was conducted with real LTE signals in a suburban environment. For this purpose, a ground vehicle was equipped with three antennas to acquire and track 1) GPS signals and 2) LTE signals in two different bands from nearby eNodeBs. The LTE antennas were consumer-grade 800/1,900-MHz cellular omnidirectional antennas, and the GPS antenna was a surveyor-grade Leica antenna. The LTE signals were simultaneously downmixed and synchronously sampled via

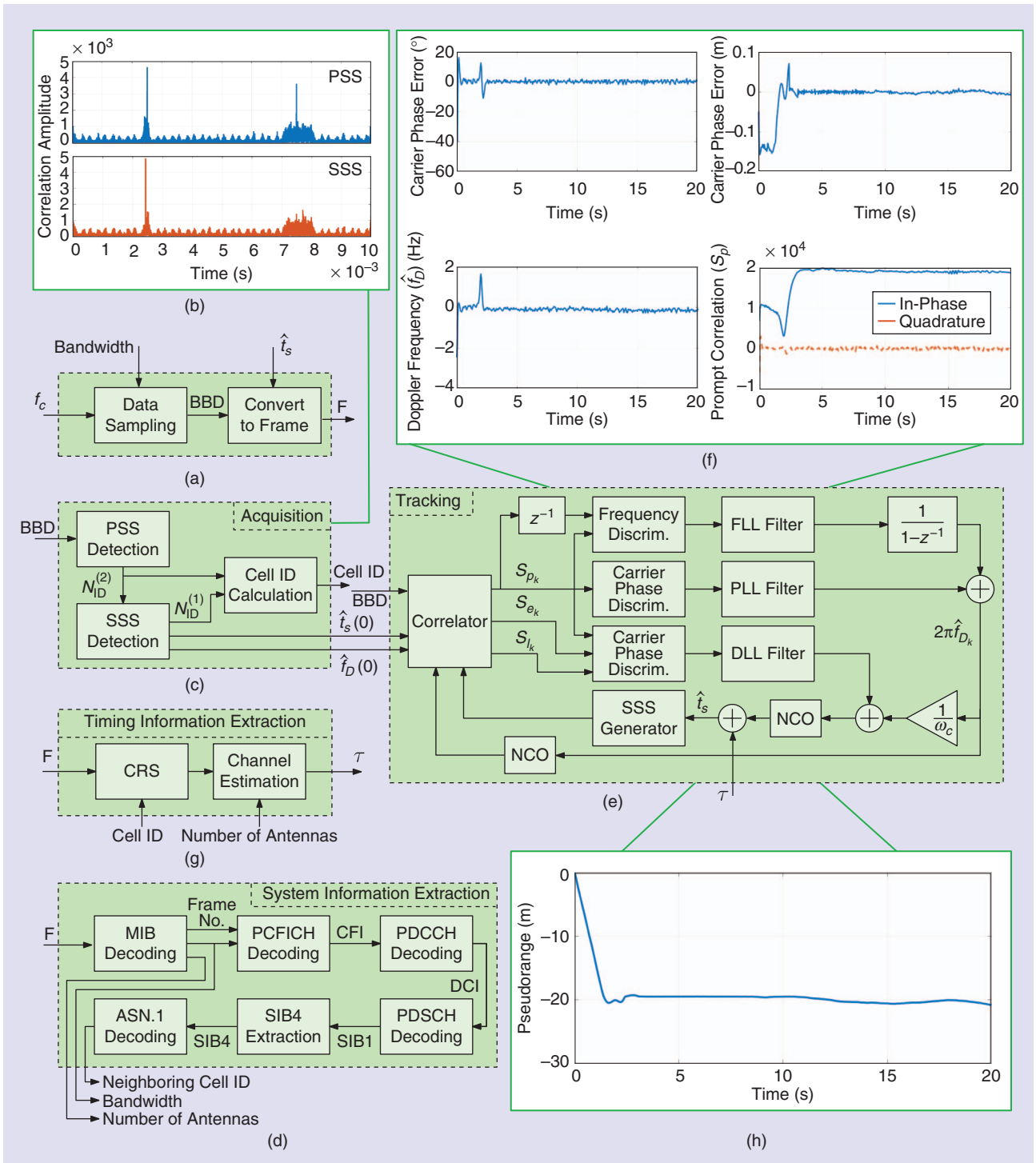

FIGURE 6. The LTE SDR architecture and results. (a) The LTE signal is 1) received by the receiver, 2) downmixed to baseband, and 3) converted to the frame structure by knowing the frame start time. (b) Correlation of the real LTE signal with PSS and SSS. (c) LTE signal acquisition. (d) Extracting relevant timing and positioning information. (e) Tracking architecture. (f) Tracking results: code and phase errors, Doppler frequency and in-phase and quadrature components of the prompt correlation. (g) Extracting high-precision frame timing by CRS. (h) Pseudorange obtained from LTE signal. F: Frame, BBD: base-band data (initial bias is removed in this figure).

a dual-channel USRP. The GPS signals were collected on a separate single-channel USRP. Over the course of the experiment, the receiver had access to LTE signals transmitted from two eNodeBs and eight GPS SVs. Due to the environment layout, the GPS signals were unobstructed; however, signals from the LTE eNodeBs experienced multipath. The LTE transmission bandwidth was measured to be 20 MHz, and the CRS signals were utilized to estimate the channel impulse response, and subsequently alleviate the multipath [41]. Samples of the received signals were stored for offline

postprocessing. The GPS signal was processed by the GRID SDR [32], and the LTE signals were processed by the LTE SDR. Figure 7(a) shows the experimental hardware and software setup. The environment layout, eNodeBs locations, and the estimated receiver trajectory from GPS and LTE signals are shown in Figure 7(b).

Figure 7(b) shows that the trajectory estimated using only LTE signals from two eNodeBs follows closely the navigation solution obtained by GPS. Poor geometric configuration of the eNodeBs is one source of error contributing to the difference between the LTE and GPS navigation solutions. By increasing the number of eNodeBs that are capable of being heard, e.g., by listening to other frequency bands and obtaining the LTE signals from other network providers, the geometric configuration could be improved. Another source of error is due to the mismatch by the velocity random walk dynamical model assumed by the EKF and the true dynamics of the vehicle. Such mismatch could be alleviated by using an INS to propagate the vehicle's states [45].

LTE versus CDMA

It is difficult to fairly compare the experimental results obtained by the CDMA and LTE signals in the "Navigation Framework and Experimental Results" sections in sections "CDMA" and "LTE," respectively, since the BTSs (eNodeBs) geometrical configuration, C/N_0, and transmitters' oscillator stability, among other parameters, are different. Nevertheless, Table 1 compares the main characteristics of 1) GPS C/A code, 2) CDMA pilot signal, and 3) three LTE reference signals (PSS, SSS, and CRS). Note that there are 63 possible PN sequences for the C/A code defined by the latest GPS Interface Specification (Interface Control Document) [46]. Table 1 shows that PSS and SSS have the worst ranging precision, which is due to their lower bandwidth. The CRS will offer the best ranging precision and will be robust to multipath due to its higher bandwidth. However, the CRS is scattered in the bandwidth, and it is not feasible to exploit conventional DLLs to track this signal. Therefore, the design of a computationally efficient receiver for navigating with the CRS remains a challenge.

Multisignal navigation: GPS and cellular

In TOA-based radio navigation, the quality of the receiver's navigation solution is determined by both the pseudorange measurement noise statistics and the spatial geometry of the transmitters. GNSS position solutions suffer from a relatively

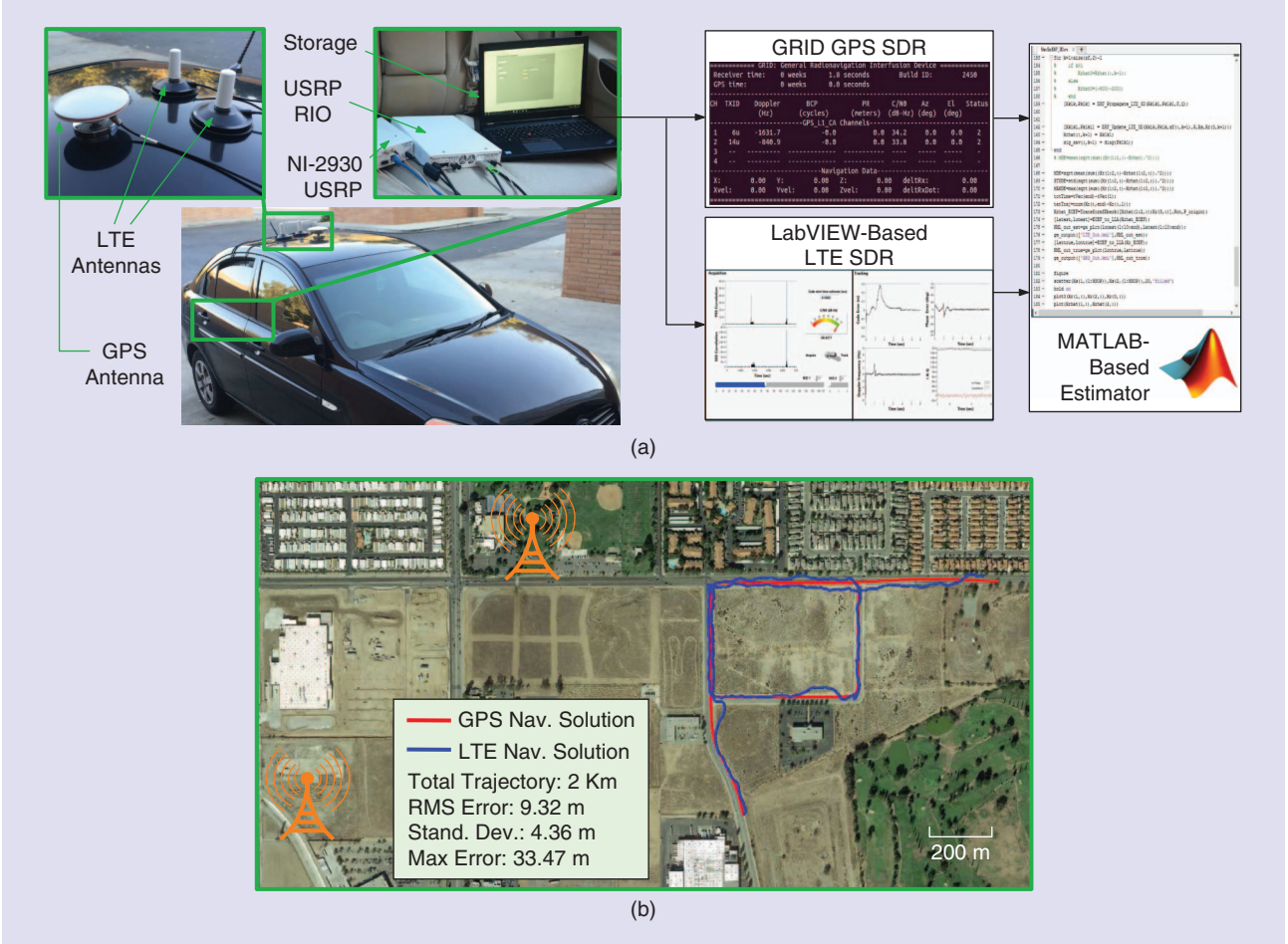

FIGURE 7. (a) The experimental setup. (b) Locations of eNodeBs and estimated receiver trajectory using GPS and LTE signals. Map data courtesy of Google Earth.

Table 1. Comparing LTE signals versus CDMA signals.

Standard	Signal	Possible number of sequences	Bandwidth (MHz)	Conventional DLLs	Code period (ms)	Expected ranging precision (m)*
GPS	C/A code	63	1.023	Yes	1	2.93
cdma2000	Pilot	512	1.2288	Yes	26.67	2.44
LTE	PSS	3	0.93	Yes	10	3.22
	SSS	168	0.93	Yes	10	3.22
	CRS	504	up to 20	No	0.067	0.15

*1% of chip width.

FIGURE 8. Experimental results comparing the navigation solution uncertainty ellipsoids produced by GPS alone and by the multisignal navigation SDR (GPS and cellular CDMA and LTE). (Map data courtesy of Google Earth.)

high vertical estimation uncertainty due to the lack of GNSS SV angle diversity (SVs are usually above the receiver). To address this, an external sensor (e.g., barometer) is typically fused with a GNSS receiver.

Terrestrial BTSs are abundant and available at varying geometric configurations unattainable by GNSS SVs (e.g., BTSs could be below a UAV-mounted receiver), making them an attractive supplement to GNSSs [47], [48]. This section presents experimental results produced by the cellular CDMA and LTE SDRs discussed previously, demonstrating the reduction in navigation solution uncertainty (particularly in the vertical) when fusing GPS and cellular signals.

Three antennas were mounted on a UAV to acquire and track GPS signals and multiple cellular BTS signals. The GPS and cellular signals were simultaneously downmixed and synchronously sampled via USRPs. These front ends fed their data to the multichannel adaptive transceiver information extractor SDR (CDMA and LTE) and GRID SDR (GPS), which produced pseudorange observables from the GPS L1 C/A signals in view and five cellular BTSs [20], [21]. Figure 8 illustrates the environment and the resulting 95th percentile uncertainty ellipsoids associated with a navigation solution using 1) seven GPS SVs and 2) seven GPS SVs along with three cellular CDMA BTSs and two LTE eNodeBs. Note that upon fusing the five cellular pseudoranges, the volume of the GPS-only navigation solution uncertainty ellipsoid V_{GPS} significantly reduced to $0.16(V_{GPS})$.

Conclusions

This article demonstrated how cellular CDMA and LTE signals could address the limitations of GNSS-based navigation. On one hand, when GNSS signals are unavailable (e.g., due to signal weakness or jamming) or untrustworthy (e.g., due to spoofing), cellular signals could be used exclusively for accurate navigation in the absence of GNSS signals. To this end, the article presented a brief overview of the forward-link channel signals in cdma2000 systems and the frame structure in LTE systems. Two SDRs were presented to extract

TOA measurements from cellular CDMA and LTE signals. Moreover, a framework for navigating exclusively with cellular signals in the case of GNSS unavailability was discussed. Experimental results were presented demonstrating a UAV navigating with cellular CDMA signals using the proposed framework and the presented CDMA SDR. An RMS position error of 9.39 m over a 512-m trajectory was achieved using only two cellular CDMA BTSs. Experimental results were presented demonstrating a ground vehicle navigating exclusively with LTE signals using the proposed LTE SDR in an environment in which the LTE signals experienced multipath. The LTE's CRS signal was utilized to estimate the channel impulse response, and subsequently alleviate the multipath. The LTE experimental results demonstrated the robustness of the proposed LTE SDR in a multipath environment. An RMS position error of 9.32 m over a 2-km trajectory was achieved using only two LTE eNodeBs.

While these experimental results do not seem impressive compared to GPS, one needs to consider several factors affecting the accuracy achieved with the experimental results presented in this article. First, due to hardware or UAV payload limitations, only two CDMA BTSs (two LTE eNodeBs) were used in the CDMA (LTE) experiments, respectively, compared to eight GPS SVs. Second, the BTS and eNodeB layout offered poor geometric diversity. Third, the vehicle dynamics (UAV and ground vehicle) were assumed to evolve according to a fixed dynamical model. Also, the statistics of the process noise driving the clock states of the vehicle-mounted SDRs, CDMA BTSs, and LTE eNodeBs were chosen according to assumed oscillator qualities, leading to dynamical and statistical model mismatches in the EKF. The navigation accuracy with cellular signals could be significantly improved by listening to more BTSs and eNodeBs, which would inherently offer better geometric diversity. Furthermore, to reduce dynamical model mismatches in the EKF, an INS could be used to propagate the position and velocity states of the UAV and ground vehicle. To reduce statistical model mismatches in the EKF, the statistics of the process noise driving the BTSs' and eNodeBs' oscillators could be characterized a priori over a long period of time or estimated on the fly via an adaptive filter [27].

On the other hand, when GNSS signals were available, the article demonstrated how exploiting the abundance and geometric diversity of cellular transmitters could significantly improve the navigation solution over that of a standalone GPS. To this end, a UAV fused pseudoranges from CDMA BTSs, LTE eNodeBs, and GPS SVs, achieving a superior navigation solution when compared to a standalone GPS, particularly in the vertical direction.

While the potential of exploiting cellular signals for accurate navigation via SDRs was demonstrated in this article, hardware and payload limitations remain a major challenge. This prevented hearing more CDMA BTSs and LTE eNodeBs in the receiver's environment. Future work could focus on optimizing the receiver to increase the number of processed signals and to reduce the size, weight, and power issues of the cellular navigation SDRs, making them embeddable on mobile devices. Moreover, this article discussed that, compared to GNSS signals, cellular signals are received at significantly higher C/N_0 and are available and usable indoors. Future work could study enabling indoor navigation via cellular signals.

Finally, by diversifying the portfolio of signals used in producing a navigation solution beyond GNSS signals, one achieves security against malicious GNSS jamming and spoofing attacks. If GNSS signals are jammed, the receiver could continue navigating with non-GNSS signals. If GNSS signals are spoofed, the receiver could detect such spoofing by cross-checking against its portfolio of signals of opportunity (e.g., cellular signals). In the future, the pursuit of GNSS spoofing detection and mitigation via cellular signals can be explored.

Acknowledgment

This work was supported in part by the Office of Naval Research under grant N00014-16-1-2305.

Authors

Zaher (Zak) M. Kassas (zkassas@ieee.org) received his B.E. degree in electrical engineering from the Lebanese American University, Beirut, in 2001, M.S. degree in electrical and computer engineering (ECE) from The Ohio State University in 2003, M.S.E. degree in aerospace engineering from the University of Texas at Austin in 2010, and Ph.D. degree in ECE from the University of Texas at Austin in 2014. From 2004 to 2010, he was a research and development engineer with the Control Design and Dynamical Systems Simulation Group at National Instruments Corp. He is an assistant professor at the University of California, Riverside, and director of the Autonomous Systems Perception, Intelligence, and Navigation Laboratory. His research interests include optimal estimation, navigation, software-defined receivers, autonomous vehicles, and intelligent transportation systems.

Joe Khalife (jkhal001@ucr.edu) received his B.E. degree in electrical engineering and M.S. degree in computer engineering from the Lebanese American University, Beirut, in 2011 and 2014, respectively. He is a Ph.D. degree student at the University of California, Riverside, and a member of the Autonomous Systems Perception, Intelligence, and Navigation Laboratory. His research interests include opportunistic navigation, autonomous vehicles, and software-defined receivers.

Kimia Shamaei (ksham002@ucr.edu) received her B.S. and M.S. degrees in electrical engineering from the University of Tehran, Iran, in 2010 and 2013, respectively. She is a Ph.D. degree candidate at the University of California, Riverside, and a member of the Autonomous Systems Perception, Intelligence, and Navigation Laboratory. Her current research interests include analysis and modeling of signals of opportunity and software-defined receivers.

Joshua Morales (jmora047@ucr.edu) received his B.S. degree in electrical and computer engineering with high honors from the University of California, Riverside, in 2014 where he is currently a Ph.D. degree student and a member of the Autonomous Systems Perception, Intelligence, and

Navigation Laboratory. His research interests include estimation, navigation, autonomous vehicles, and intelligent transportation systems.

References

[1] G. Seco-Granados, J. Lopez-Salcedo, D. Jimenez-Banos, and G. Lopez-Risueno, "Challenges in indoor global navigation satellite systems: Unveiling its core features in signal processing," *IEEE Signal Process. Mag.*, vol. 29, no. 2, pp. 108–131, Mar. 2012.

[2] J. Grabowski, "Personal privacy jammers: Locating Jersey PPDs jamming GBAS safety-of-life signals," *GPS World Mag.*, vol. 23, no. 4, pp. 28–37. Apr. 2012.

[3] C. Günther, "A survey of spoofing and counter-measures," *J. Inst. Navigat.*, vol. 61, no. 3, pp. 159–177, 2014.

[4] P. Misra and P. Enge, *Global Positioning System: Signals, Measurements, and Performance*, 2nd ed. Lincoln, MA: Ganga-Jamuna Press, 2010.

[5] Z. Kassas, "Collaborative opportunistic navigation," *IEEE Aerospace Electron. Syst. Mag.*, vol. 28, no. 6, pp. 38–41, 2013.

[6] J. McEllroy, "Navigation using signals of opportunity in the AM transmission band," M.S. thesis, Dept. Electrical and Computer Engineering, Air Force Inst. Technol., Wright-Patterson Air Force Base, OH, 2006.

[7] S. Fang, J. Chen, H. Huang, and T. Lin, "Is FM a RF-based positioning solution in a metropolitan-scale environment? A probabilistic approach with radio measurements analysis," *IEEE Trans. Broadcast.*, vol. 55, no. 3, pp. 577–588, Sept. 2009.

[8] M. Joerger, L. Gratton, B. Pervan, and C. Cohen, "Analysis of Iridium-augmented GPS for floating carrier phase positioning," *J. Inst. Navigat.*, vol. 57, no. 2, pp. 137–160, 2010.

[9] K. Pesyna, Z. Kassas, and T. Humphreys, "Constructing a continuous phase time history from TDMA signals for opportunistic navigation," in *Proc. IEEE/ION Position Location and Navigation Symp.*, Apr. 2012, pp. 1209–1220.

[10] K. Pesyna, Z. Kassas, J. Bhatti, and T. Humphreys, "Tightly-coupled opportunistic navigation for deep urban and indoor positioning," in *Proc. ION GNSS Conf.*, Sept. 2011, pp. 3605–3617.

[11] C. Yang, T. Nguyen, and E. Blasch, "Mobile positioning via fusion of mixed signals of opportunity," *IEEE Aerospace Electron. Syst. Mag.*, vol. 29, no. 4, pp. 34–46, Apr. 2014.

[12] M. Rabinowitz and J. Spilker, Jr., "A new positioning system using television synchronization signals," *IEEE Trans. Broadcast.*, vol. 51, no. 1, pp. 51–61, Mar. 2005.

[13] P. Thevenon, S. Damien, O. Julien, C. Macabiau, M. Bousquet, L. Ries, and S. Corazza, "Positioning using mobile TV based on the DVB-SH standard," *J. Inst. Navigat.*, vol. 58, no. 2, pp. 71–90, 2011.

[14] J. Biswas and M. Veloso, "WiFi localization and navigation for autonomous indoor mobile robots," in *Proc. IEEE Int. Conf. Robotics and Automation*, May 2010, pp. 4379–4384.

[15] J. Khalife, Z. Kassas, and S. Saab, "Indoor localization based on floor plans and power maps: Non-line of sight to virtual line of sight," in *Proc. ION GNSS Conf.* Sept. 2015, pp. 2291–2300.

[16] F. Principe, G. Bacci, F. Giannetti, and M. Luise, "Software-defined radio technologies for GNSS receivers: a tutorial approach to a simple design and implementation," *Int. J. Navigat. Observ.*, vol. 2011, article ID 979815.

[17] C. Fernandez-Prades, J. Arribas, P. Closas, C. Aviles, and L. Esteve, "GNSS-SDR: An open source tool for researchers and developers," in *Proc. ION GNSS Conf,.* Sept. 2011, pp. 780–794.

[18] G. Hamza, A. Zekry, and I. Motawie, "Implementation of a complete GPS receiver using Simulink," *IEEE Circuits Syst. Mag.*, vol. 9, no. 4, pp. 43–51, 2009.

[19] Z. Kassas, J. Bhatti, and T. Humphreys, "A graphical approach to GPS software-defined receiver implementation," in *Proc. IEEE Global Conf. Signal and Information Processing.,* Dec. 2013, pp. 1226–1229.

[20] J. Khalife, K. Shamaei, and Z. Kassas, "A software-defined receiver architecture for cellular CDMA-based navigation," in *Proc. IEEE/ION Position, Location, and Navigation Symp.*, Apr. 2016, pp. 816–826.

[21] K. Shamaei, J. Khalife, and Z. Kassas, "Performance characterization of positioning in LTE systems," in *Proc. ION GNSS Conf.*, Sept. 2016, pp. 2262–2270.

[22] "Physical layer standard for CDMA2000 spread spectrum systems," Revision E, Rep. C.S0002-E3 GPP2, June 2011. [Online]. Available: http://www.3gpp2.org/Public_html/Specs/C.S0002-E_v3.0_cdma2000_1x_PHY_20110620.pdf

[23] "Upper layer (layer 3) signaling standard for CDMA2000 spread spectrum systems," Rep. C.S0005-F v2.0, May 2014. [Online]. Available: http://www.arib.or.jp/english/html/overview/doc/STD-T64v6_80/Specification/ARIB_STD-T64-C.S0005-Fv2.0.pdf

[24] D. van Nee and A. Coenen, "New fast GPS code-acquisition technique using FFT," *Electron. Lett.*, vol. 27, no. 2, pp. 158–160, Jan. 1991.

[25] E. Kaplan and C. Hegarty, *Understanding GPS: Principles and Applications*, 2nd ed. Norwood, MA: Artech House, 2005.

[26] "Universal mobile telecommunications system (UMTS): Base station (BS) radio transmission and reception (FDD)," ETSI, ETSI TS 125 104 v12.5.0, 2015. [Online]. Available: http://www.etsi.org/deliver/etsi_ts/125100_125199/125104/12.05.00_60/ts_125104v120500p.pdf

[27] Z. Kassas, V. Ghadiok, and T. Humphreys, "Adaptive estimation of signals of opportunity," in *Proc. ION GNSS Conf.*, Sept. 2014, pp. 1679–1689.

[28] J. Morales and Z. Kassas, "Optimal receiver placement for collaborative mapping of signals of opportunity," in *Proc. ION GNSS Conf.*, Sept. 2015, pp. 2362–2368.

[29] M. Bshara, U. Orguner, F. Gustafsson, and L. Van Biesen, "Robust tracking in cellular networks using HMM filters and cell-ID measurements," *IEEE Trans. Veh. Technol.*, vol. 60, no. 3, pp. 1016–1024, Mar. 2011.

[30] Z. Abu-Shaban, X. Zhou, and T. Abhayapala, "A novel TOA-based mobile localization technique under mixed LOS/NLOS conditions for cellular networks," *IEEE Trans. Veh. Technol.*, vol. 65, no. 11, pp. 8841–8853, 2016.

[31] K. Carter, R. Ramlall, M. Tummala, and J. McEachen, "Bandwidth efficient ATSC TDOA positioning in GPS-denied environments," in *Proc. ION Int. Tech. Meeting Conf.*, Jan. 2013, pp. 717–725.

[32] T. Humphreys, J. Bhatti, T. Pany, B. Ledvina, and B. O'Hanlon, "Exploiting multicore technology in software-defined GNSS receivers," in *Proc. ION GNSS Conf.*, Sept. 2009, pp. 326–338.

[33] Z. Kassas and T. Humphreys, "Observability analysis of collaborative opportunistic navigation with pseudorange measurements," *IEEE Trans. Intell. Transport. Syst.*, vol. 15, no. 1, pp. 260–273, Feb. 2014.

[34] J. del Peral-Rosado, J. Lopez-Salcedo, G. Seco-Granados, F. Zanier, P. Crosta, R. Ioannides, and M. Crisci, "Software-defined radio LTE positioning receiver towards future hybrid localization systems," in *Proc. Int. Commun. Satellite Systems Conf.*, Oct. 2013, pp. 14–17.

[35] J. del Peral-Rosado, J. Parro-Jimenez, J. Lopez-Salcedo, G. Seco-Granados, P. Crosta, F. Zanier, and M. Crisci, "Comparative results analysis on positioning with real LTE signals and low-cost hardware platforms," in *Proc. Satellite Navigation Technologies and Eur. Workshop GNSS Signals and Signal Processing*, Dec. 2014, pp. 1–8.

[36] F. Knutti, M. Sabathy, M. Driusso, H. Mathis, and C. Marshall, "Positioning using LTE signals," in *Proc. Eur. Navigation Conf.*, Apr. 2015, pp. 1–8.

[37] M. Driusso, F. Babich, F. Knutti, M. Sabathy, and C. Marshall, "Estimation and tracking of LTE signals time of arrival in a mobile multipath environment," in *Proc. Int. Symp. Image and Signal Processing and Analysis.,* Sept. 2015, pp. 276–281.

[38] M. Ulmschneider and C. Gentner, "Multipath assisted positioning for pedestrians using LTE signals," in *Proc. IEEE/ION Position, Location, and Navigation Symp.*, Apr. 2016, pp. 386–392.

[39] C. Chen and W. Wu, "Three-dimensional positioning for LTE systems," *IEEE Trans. Veh. Technol.*, vol. 66, no. 4, pp. 3220–3234, Apr. 2017.

[40] M. Driusso, C. Marshall, M. Sabathy, F. Knutti, H. Mathis, and F. Babich, "Vehicular position tracking using LTE signals," *IEEE Trans. Veh. Technol.*, vol. 66, no. 4, pp. 3376–3391, Apr. 2017.

[41] K. Shamaei, J. Khalife, and Z. Kassas, "Comparative results for positioning with secondary synchronization signal versus cell specific reference signal in LTE systems," in *Proc. ION Int. Tech. Meeting Conf.*, Jan. 2017, 1256–1268.

[42] Evolved universal terrestrial radio access (E-UTRA): Physical channels and modulation; 3rd Generation Partnership Project (3GPP). Rep. TS 36.211. (2011, Jan.). [Online]. Available: http://www.3gpp.org/ftp/Specs/html-info/36211.htm

[43] M. Hofer, J. McEachen, and M. Tummala, "Vulnerability analysis of LTE location services," in *Proc. Hawaii Int. Conf. System Sci.*, Jan. 2014, pp. 5162–5166.

[44] J. van de Beek, M. Sandell, and P. Borjesson, "ML estimation of time and frequency offset in OFDM systems," *IEEE Trans. Signal Process.*, vol. 45, no. 7, pp. 1800–1805, July 1997.

[45] J. Morales, P. Roysdon, and Z. Kassas, "Signals of opportunity aided inertial navigation," in *Proc. ION GNSS Conf.*, Sept. 2016, pp. 1492–1501.

[46] Space segment/navigation user interfaces interface specification IS-GPS-200. Navstar GPS. (2015, Dec.). [Online]. Available: http://www.gps.gov/technical/icwg/

[47] J. Morales, J. Khalife, and Z. Kassas, "GNSS vertical dilution of precision reduction using terrestrial signals of opportunity," in *Proc. ION Int. Tech. Meeting Conf.*, Jan. 2016, pp. 664–669.

[48] "Opportunity for accuracy," *GPS World Mag.*, vol. 27, no. 3, pp. 22–29, Mar. 2016.

SP